Materials Today Bio 20 (2023) 100616

Contents lists available at ScienceDirect

Materials Today Bio

journal homepage: www.journals.elsevier.com/materials-today-bio

Photocatalytic oxygen evolution and antibacterial biomimetic repair membrane for diabetes wound repair via HIF1-α pathway

Yanlin Su [a,1], Bing Ye [a,1], Ziming Zhang [e,1], Qing Gao [a], Lian Zeng [a], Yizhou Wan [a], Wenzhe Sun [a], Siyue Chen [d], Daping Quan [b,***], Jialin Yu [c,**], Xiaodong Guo [a,*]

[a] Department of Orthopedics, Union Hospital, Tongji Medical College, Huazhong Univer sity of Science and Technology, Wuhan, Hubei, 430022, China
[b] PCFM Lab, School of Chemistry and School of Materials Science and Engineering, Sun Yat-sen University, Guangzhou, Guangdong, 510000, China
[c] The First Affiliated Hospital of Yangtze University, Jingzhou, Hubei, 430022, China
[d] School of Basic Medicine, Tongji Medical College, Huazhong University of Science and Technology, Wuhan, Hubei, 430022, China
[e] Department of Orthopedics, Zaoyang First People's Hospital, Zaoyang, Hubei, 430022, China

ARTICLE INFO

Keywords:
Diabetic wound repair
Photocatalysis
Oxygen evolution
Antibacterial
Fibroblast
Neurovascular

ABSTRACT

Diabetic wounds always have puzzled patients and caused serious social problems. Due to the lack of local blood vessels, severe hypoxia is generated in the defect area, which is an essential reason for the difficulty of wound healing. We have constructed a photocatalytic oxygen evolution and antibacterial biomimetic repair membrane to solve the problems of wound repair. A scanning electron microscope and transmission electron microscope characterized the biomimetic repair membrane. The oxygen evolution of the biomimetic membrane was tested by an oxygen meter. The excellent antibacterial performance of the biomimetic repair membrane was also verified by co-culture with *Staphylococcus aureus* and *Escherichia coli*. It was confirmed that the expression of collagen and HIF1-α in fibroblasts was significantly increased in vitro. And the mitochondrial activity of the vascular and nerve was increased considerably. In vivo, the healing time of diabetes wounds treated with the biomimetic repair membrane was significantly reduced, the collagen and the number of pores were increased considerably, and vascular regeneration was enhanced. The biomimetic repair membrane has an excellent performance in photocatalytic oxygen evolution and antibacterial and can significantly promote the repair of diabetes wounds. This will provide a promising treatment for diabetes wound repair.

1. Introduction

Diabetic wound healing is a complex and severe clinical challenge that affects approximately 10% of the population in world [1]. There are many reasons for undesirable wound healing in diabetes: barrier destruction, neuropathy, and inflammation [2,3]. Local hypoxia and bacterial infection are crucial factors [4].

Oxygen can effectively promote local cell proliferation and metastasis, angiogenesis, and other repair processes in the wound [5]. Mitochondria are the main places for aerobic cell respiration, and its matrix and intima participate in the last two stages of aerobic respiration (tricarboxylic acid cycle and oxidative phosphorylation). And releasing a large amount of ATP can provide a good energy supply [6]. In addition, some studies have found that the regulation of mitochondrial morphology plays a vital role in the process of apoptosis. The morphology of mitochondria can also control stem cell regeneration by regulating protein homeostasis and metabolism. The number and shape of mitochondria are vital target spots for cell respiration and energy supply [7,8]. However, due to vascular damage, critical oxygen cannot be delivered to the wound tissue [9]. On the other hand, high blood sugar can cause systemic inflammation, leading to neutrophil functional defects under long-term stress [10]. People with diabetes are more likely to develop bacterial infections due to disorders of the immune system, longer healing cycles, and moist skin wounds [11,12]. Hypoxia and bacterial infections can lead to more severe local inflammation. In this abnormal microenvironment, endothelial cell dysfunction and

* Corresponding author.
** Corresponding author.
*** Corresponding author.
E-mail addresses: cesqdp@mail.sysu.edu.cn (D. Quan), 2021710955@yangtzeu.edu.cn (J. Yu), xiaodongguo@hust.edu.cn (X. Guo).
[1] These authors contributed equally.

https://doi.org/10.1016/j.mtbio.2023.100616
Received 20 January 2023; Received in revised form 26 February 2023; Accepted 19 March 2023
Available online 23 March 2023
2590-0064/© 2023 The Authors. Published by Elsevier Ltd. This is an open access article under the CC BY-NC-ND license (http://creativecommons.org/licenses/by-nc-nd/4.0/).

angiogenesis are impaired [13,14]. Currently, antibiotics are the most common way to treat bacterial infections in the clinic. However, due to the resistance of many bacteria to antibiotics and the emergence of multidrug-resistant (MDR) bacteria, antibiotics often fail to achieve the desired effect [15,16]. This seriously hinders wound healing in patients with diabetes. Therefore, we urgently need a dressing that can produce oxygen and an efficient antibacterial effect as an effective strategy to deal with the microenvironment of local hypoxia and bacterial infection in diabetic wounds.

Sensory and autonomic nerves are present in the skin, and sensory nerves are widely distributed and dominant in the skin [17]. The dense network of sensory nerve afferents and neuromodulators in the skin is communicated bidirectionally with epidermal keratinocytes and dermal fibroblasts, which play an essential wound healing after trauma. In addition, some studies have found that the decrease in dermal vascularization expressing VEGFR is associated with neurological abnormalities in diabetes [18–20]. Therefore, for the healing of diabetic wounds, sensory nerves have an essential role.

MXene is an up-and-coming reducing agent that can help anesis excessive local oxidative stress [21]. Moreover, MXene has excellent biocompatibility, photo response property, photocatalytic performance, low cytotoxicity, excellent photothermal conversion efficiency, and exhibits perfect antimicrobial activity [22–27]. Some studies have found that MXene also significantly promotes angiogenesis [28,29]. Therefore, MXene is suitable for relieving oxidative stress in diabetic wounds and has excellent potential to be used in diabetic wounds.

Polyaniline (PANI) is a conductive polymer with simple synthesis, excellent carrier mobility, and good electrical conductivity [30,31]. Due to the superb carrier mobility of PANI. The combination of PANI and MXene is beneficial to the faster separation of photogenerated carriers [32], which can improve the photocatalytic performance of MXene. Under the photocatalysis of materials, water can be decomposed to produce oxygen [33]. The oxygen released can effectively alleviate the local hypoxia of the wound [34]. In addition, PANI also helps to improve the stability of MXene [35]. As an outstanding polymer, PANI will play an excellent role in combining with MXene. To provide a grandiose scheme for relieving local hypoxia of diabetic wounds.

In this experiment, we would design a biomimetic membrane with photocatalytic oxygen production, photothermal antibacterial, and neuroangiogenic activities. The first step in constructing our biomimetic membrane is to prepare the PCL (poly (ε-caprolactone)) membrane by electrospinning. Then, we loaded the MXene@PANI heterojunction onto the biomimetic membrane through collagen II. Afterward, NGF and VEGF were loaded on the biomimetic membrane with PEI. Finally, a multi-functional photocatalytic biomimetic repair membrane (PMP@GFs) was formed. In this design, MXene provides photothermal antimicrobial efficacy; PANI works with MXene under near-infrared light to produce oxygen. Moreover, the release of VEGF and NGF can synergistically promote effective wound neurovascular regeneration. The resulting blood vessels can meet the continuous oxygen supply to the tissue. PMP@GFs biomimetic repair membrane will demonstrate photocatalytic oxygen release and the antibacterial ability for diabetic wound healing. On the other hand, it will promote the regeneration of nerves and blood vessels. In conclusion, photocatalytic biomimetic repair membrane offers new prospects for treating diabetic wounds (Scheme 1).

2. Materials and methods

2.1. Preparation of MXene@PANI heterostructure by ultrasonic method

According to previous reports [36], we prepared MxeneTi3C2Tx by acid etching. Then the MXene powder was added to isopropanol (IPA) and treated by ultrasonic for 2 h. After the ultrasonic treatment, we centrifuged it for 20min (4000RMP). Get a few layers of MXene. The heterojunctions of Polyaniline (P838554, Shanghai Macklin Biochemical Technology Co., Ltd. Shanghai, China) and few-layer MXene were synthesized by electrostatic interaction after ultrasonic for 3 h.

2.2. Characterization

We used scanning electron microscopy (SEM, Zeiss Sigma 300; Carl Zeiss AG, Jena, Germany) to observe the bystander morphology of the material. After fixing the fabric, wash it with PBS, dehydrate it with ethanol gradient, mix it with isoamyl acetate and ethanol (V/V = 1/1) for 30 min, and then treat it with pure isoamyl acetate for 1 h. Drying at the critical point, coating with gold powder, and finally observing by scanning electron microscope. The heterostructure was observed by transmission electron microscopy (TEM; JEM-2100F, JEOL, Tokyo, Japan).

2.3. Electrospinning and collagen-loaded heterostructure

We added PCL particles (12%w/v) into TFEA (2,2,2-trifluoroethanol) to prepare the PCL solution. Driven by a syringe pump, the solution was pumped with a 10 ml syringe through a spinneret at a constant flow rate (Q = 0.1 ml/min) to prepare nanofibers. Then, the DC power supply of the voltage regulator (Tonli, Shenzhen, China) was connected, and electrospinning was carried out after applying a high voltage (13 kV). The nanofibers were arranged vertically, electrospinning was carried out on the copper roller, and the spinneret and collector were set to 10 cm spacing. The copper roller (diameter 15 cm, width 10 mm) is connected to a negative voltage of 1.5 kV to rotate (3000 rpm). For sterilization, put the prepared membrane in 70% ethanol for 3 h.

2.4. Absorption spectrum

The 0.5 cm × 0.5 cm biomimetic repair membrane was placed in the glass micropore of a 96-well quartz enzyme plate and laid at the bottom. Using the Multiskan Spectrum (Thermo Fisher Scientific, Waltham, MA, USA) to set from 300 to 1000 nm, each 30 nm was detected, and the absorption spectrum was recorded and drawn using GraphPad Prism.

2.5. Photoelectric detection

The electrochemical workstation Zahner PP211 (Germany) was used to evaluate the photoelectric response of MXene@PANI. To coat MXene@PANI on ITO (indium tin oxide), which served as the photoanode, sodium sulfate was used as the electrolyte, a platinum wire as the cathode, and saturated calomel as the reference electrode. Near-infrared laser (808 nm) was placed at 20 cm as the light source. The linear sweep voltammograms of different samples were measured at a scanning rate of 10 MV s-1.

2.6. Photothermal detection

To evaluate the photothermal performance of the biomimetic repair membrane, we used a near-infrared laser of 808 nm (BWT, Beijing, China) to irradiate the biomimetic repair membrane for 5 min, and the temperature change was carefully recorded by the American FLIR C2 near-infrared thermal imager. Then, we evaluated the photothermal stability of the fiber membrane and recorded the temperature change of biomimetic membranes under 808 nm near-infrared radiation. Subsequently, we tested the film's tensile strength after five near-infrared radiation cycles.

2.7. Dissolved oxygen detection

First, put the biomimetic repair membrane in water. After 30 min of near-infrared light irradiation, we used a portable dissolved oxygen

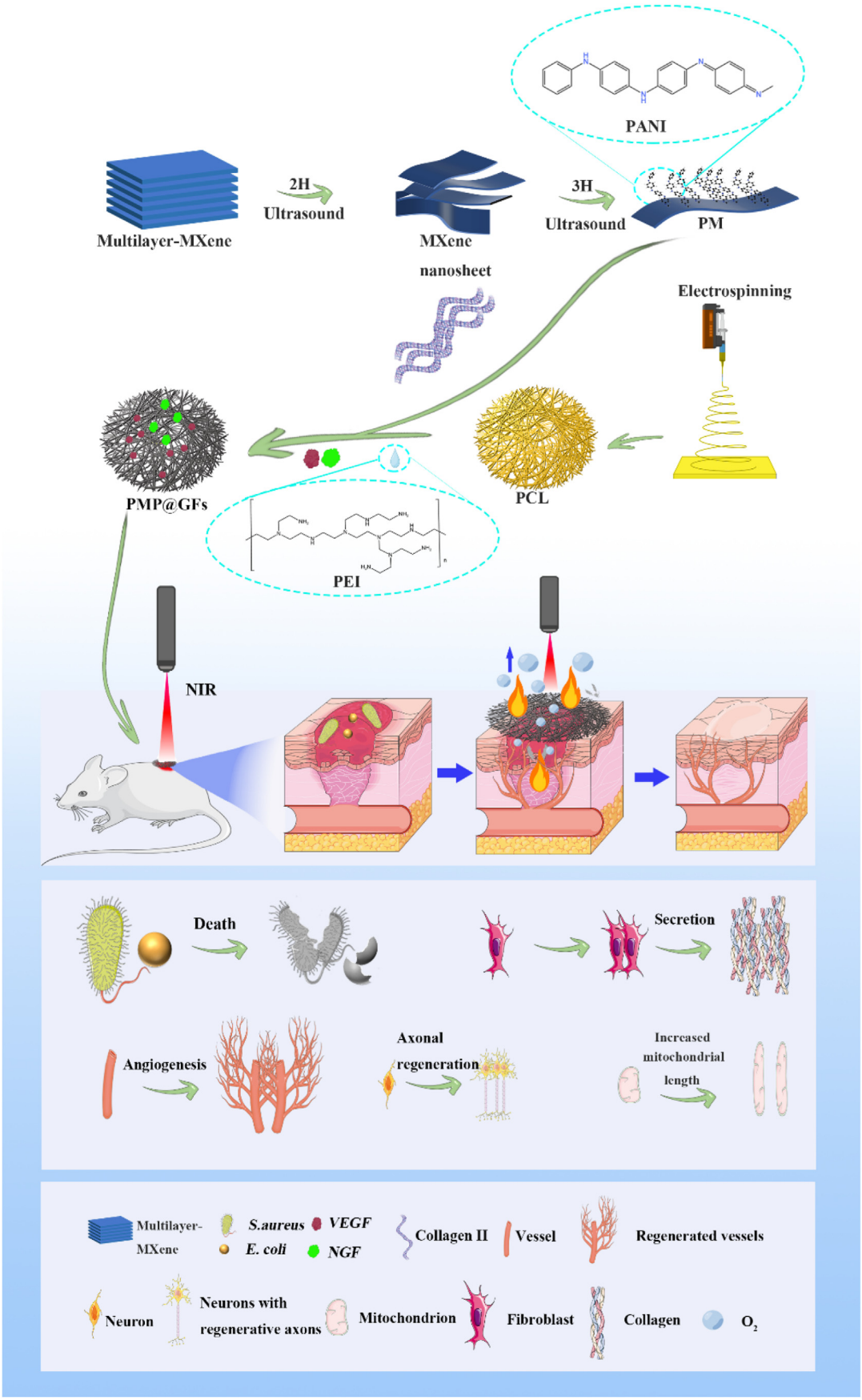

Scheme 1. Schematic diagram of Photocatalytic Oxygen Evolution and Antibacterial biomimetic repair membrane for treatment of Diabetes wound.

detector (JPB-607A, Leici, Shanghai, China) to detect the dissolved oxygen in the water. Clean the electrode with distilled water before testing. The reading of the instrument dial is the dissolved oxygen concentration.

2.8. Antibacterial detection

First, we inoculate some bacteria (*Escherichia coli* and *Staphylococcus aureus*) into an LB medium with an inoculation ring and culture for 24 h. After obtaining the bacterial solution, we will co-culture the bionic repair film with the bacterial solution for 24 h. Remove the material, suck out the bacterial solution, and dilute it to a concentration of 10 ˆ-5. The bacterial solution was dispersed on the prepared LB solid medium to observe the antibacterial effect after 24 h of cultivation. Use ImageJ to carry out statistical analysis on colonies.

2.9. Biofilm detection

Add PCL membrane and PMP@GFs biomimetic membranes to the 96-well culture plate and add 100 μl culture medium, inoculate 10 μl bacterial solution, incubate at 37 °C for 36 h, then suck out the culture medium, rinse each well with 200 μl aseptic PBS buffer for 3 times, fix 15min after adding 100 μl methanol, then suck out the methanol from the culture hole and air dry naturally; add 100 μl crystal violet solution and dye 5min at room temperature. After sucking out the crystal violet dye solution from the culture hole, it was dried in an oven at 37 °C. After thoroughly drying, 100 μl 13% glacial acetic acid solution was added to each hole, and the crystal violet was dissolved for 30min in the incubator at 37 °C. Finally, an enzyme labeling instrument determined the OD value of the key in the culture hole. A fluorescence microscope (X71, Olympus, Japan) was used to take pictures. The samples were quantitatively analyzed by ImageJ software (NIH, Bethesda, MD, USA).

2.10. Immunofluorescence

In short, paraffin-embedded tissue sections are dewaxed and hydrated in a series of xylene and ethanol solutions. The cells were blocked with the corresponding serum of the second antibody for 1 h and incubated with the first antibody (NF200, ab134306, Abcam, USA), (CD31, ab28364, Abcam, USA), (Vimentin (VIM), ab8978, Abcam, USA), (col I, ab96723, Abcam, USA), (col III, ab23445, Abcam, USA) overnight. Finally, histological images were observed and collected under a fluorescence microscope (X71, Olympus, Japan). The samples were quantitatively analyzed by ImageJ software (NIH, Bethesda, MD, USA).

2.11. Oxygen probe

HUVEC, PC12, NIH3T3 were inoculated on a 96-well plate, and the cells were chemically anoxic for 4 h, then [Ru (DPP) $_3$] Cl_2 (P48392, Huaxia Reagent Co., Ltd., Sichuan, China) was added to each well. After 2 h of treatment, PBS was cleaned, then biomimetic membranes were added into the hole and incubated for 4 h. After PBS cleaning, the fluorescence of the cells was observed by 594 nm and photographed with a fluorescence microscope.

2.12. JC-1detection

HUVEC, PC12, and NIH3T3 were cultured in a medium containing PMP@GFs biomimetic membranes for 4 h. The culture medium was aspirated, washed with PBS, and 1 ml of cell culture medium was added. Then add 1 ml of JC-1 staining working solution and mix thoroughly. Place in a constant temperature cell culture incubator at 37 °C for 20 min. After incubation, aspirate the supernatant, wash twice with JC-1 staining buffer, and add 2 ml of cell culture medium. Observe the fluorescence change of JC-1 with a fluorescence microscope.

2.13. Establishment of diabetic facial mouse model

The rats were anesthetized by intraperitoneal injection of 1% pentobarbital sodium. All operations were carried out under aseptic conditions. Firstly, the hair on the back of diabetic mice was shaved off with a shaver. The diabetic rats were fixed, and the surgical area was disinfected with 75% medical alcohol. Secondly, two round full-thickness skin wounds with a diameter of 1.5 cm were made on the back of each rat. The rats after the operation were randomly divided into three groups: (n = 5): PCL, PMP, and PMP@ GFs group.

2.14. HE, MASSON

We removed and collected the regenerated skin samples of rats on the 14th day. Simply put, prepare 4 micr4-microns for hue and Masson trichromatic staining. All sections were analyzed and photographed with a microscope (X71, Olympus, Japan).

2.15. Statistical analysis

The above data are statistically analyzed by GraphPad software (GraphPad Software, San Diego, CA, USA) and expressed as mean ± standard deviation (SD). Tukey's post hoc test analyzed the statistical significance between groups. The unpaired double-tailed *t*-test was used for intergroup analysis. The value of $p < 0.05$ was considered to be statistically significant. $^{*}p < 0.05$, $^{**}p < 0.01$, $^{***}p < 0.001$, and $^{****}p < 0.0001$.

3. Results

3.1. Synthesis and characterization of PMP@GFs biomimetic membranes

We use the ultrasonic method to synthesize the purchased organ-mounted MXene into a few layers of two-dimensional MXene. Then we mix the two-dimensional MXene with polyaniline through the ultrasonic process to construct MXene@PANI Heterostructure. It can be seen that the few layers of MXene have been successfully synthesized (Fig. 1. A), and PANI is successfully combined with a few layers of MXene (Fig. 1. B). The heterostructure was successfully synthesized for further verification of MXene@PANI, and TEM scanning was performed. Fig. 1. C is the TEM image of a few layers of MXene; Fig. 1D shows that PANI is loaded on single-layer MXene. And EDS-mapping is performed simultaneously, MXene @PANI Heterostructure EDS-mapping shows C/N/Ti elements (Fig. 1 E-I). The quantitative statistical chart of the elements of the tangent line of Fig. 1. I (Fig. 1. J). The above results confirm that we successfully synthesized MXene@PANI Heterostructure.

Subsequently, we use collagen II to combine the electrospun PCL biomimetic membrane with MXene@PANI Heterojunction. We use SEM to characterize the biomimetic membrane. Fig. 2. A is PCL electrospun membrane (PCL), PCL electrospun membrane loaded with few layers of MXene (PM) (Fig. 2. B), and loaded MXene@PANI Heterostructure and electrospun membrane of vascular endothelial growth factor (VEGF)and nerve growth factor (NGF) (PMP@GFs) (Fig. 2. C). Subsequently, EDS-Mapping was used to analyze the elements of the synthesized photocatalytic biomimetic membrane. (Fig. 2 D-H). The above results show that we successfully synthesized PMP@GFs.

3.2. Performance of photocatalytic biomimetic membrane

Next, we will test the performance of the biomimetic membrane. First, we carried out absorption spectrum detection. The absorption spectrum of the MXene@PANI heterostructure increases in Near-infrared wavelength (Fig. 2. I). And then, the absorption spectrum of PMP@GFs biomimetic membrane increased obviously in the near-infrared light (Fig. 2. J). Later, the MXene@PANI Heterostructure can generate photocurrent in the presence of a near-infrared laser. The above

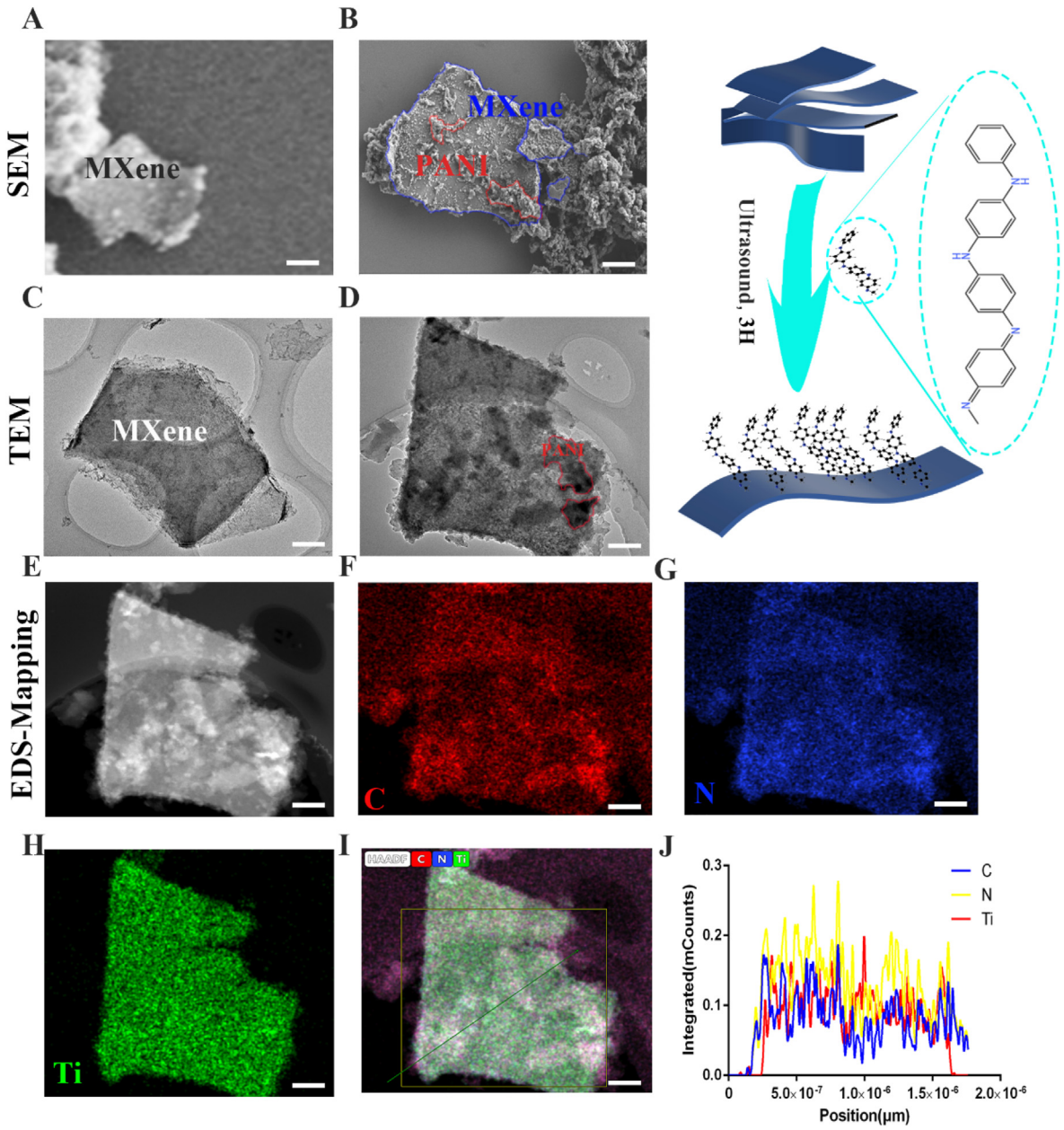

Fig. 1. Characterization of MXene@PANI heterojunction (A) The scanning electron microscope of MXene, (B) The scanning electron microscope of MXene@PANI, (C) The transmission electron microscope of MXene, (D) The transmission electron microscope of MXene@PANI, (E–I) The EDS-mapping of MXene@PANI, (J) Section element content of MXene@PANI. Scale bar = 200 nm.

experiments can show that the biomimetic membrane can absorb more photons in the near-infrared light region. The photoelectric effect is then used to generate a photoelectric current (Fig. 2. K).

The photothermal effect plays a vital role in antibacterial activity. Later, we also tested the photothermal effect of the PMP@GFs biomimetic membrane. The temperature reached 52 °C within 9s, while the temperature of the PCL group was about 30 °C. And reduce to the original temperature within 6 s (Fig. 3. A-F, H). We also conducted the oxygen evolution experiment of the bionic repair membrane, and the oxygen production of the bionic repair membrane can reach 6.6 mg/L ((Fig. 3. G).

3.3. Antibacterial effect of the PMP@GFs biomimetic membrane

For diabetic wound healing, bacterial infection will seriously hinder wound healing. Therefore, the antibacterial performance of the PMP@GFs biomimetic membrane was tested. We co-culture *Staphylococcus aureus* and *Escherichia coli* with biomimetic repair membranes. The deadly effects of PMP@GFs biomimetic membrane on *Staphylococcus aureus* shows that the killing efficiency of the biomimetic membrane against *Staphylococcus aureus* has reached 95% (Fig. 4. A and K). Similarly, the fatal effects of the PMP@GFs biomimetic membrane on *Escherichia coli* and the killing efficiency of the PMP@GFs biomimetic membrane on *Escherichia coli* also reached 98% (Fig. 4. B and L). Later, the anti-bacterial biofilm performance of the PMP@GFs biomimetic membrane was tested. It can be seen that the PMP@GFs biomimetic membrane has been reduced to 0.17 times that of the PCL group (Fig. 4. C, G, and M). PMP@GFs Biomimetic bacterial membrane biofilm formation has decreased to 0.15 times that of the PCL group (Fig. 4. D. H and N). To observe the changes of bacteria cultured on PMP@GFs biomimetic membrane. We use scanning electron microscopy to monitor the cultured bacteria. It can be seen that the surface of *Staphylococcus aureus* is broken.

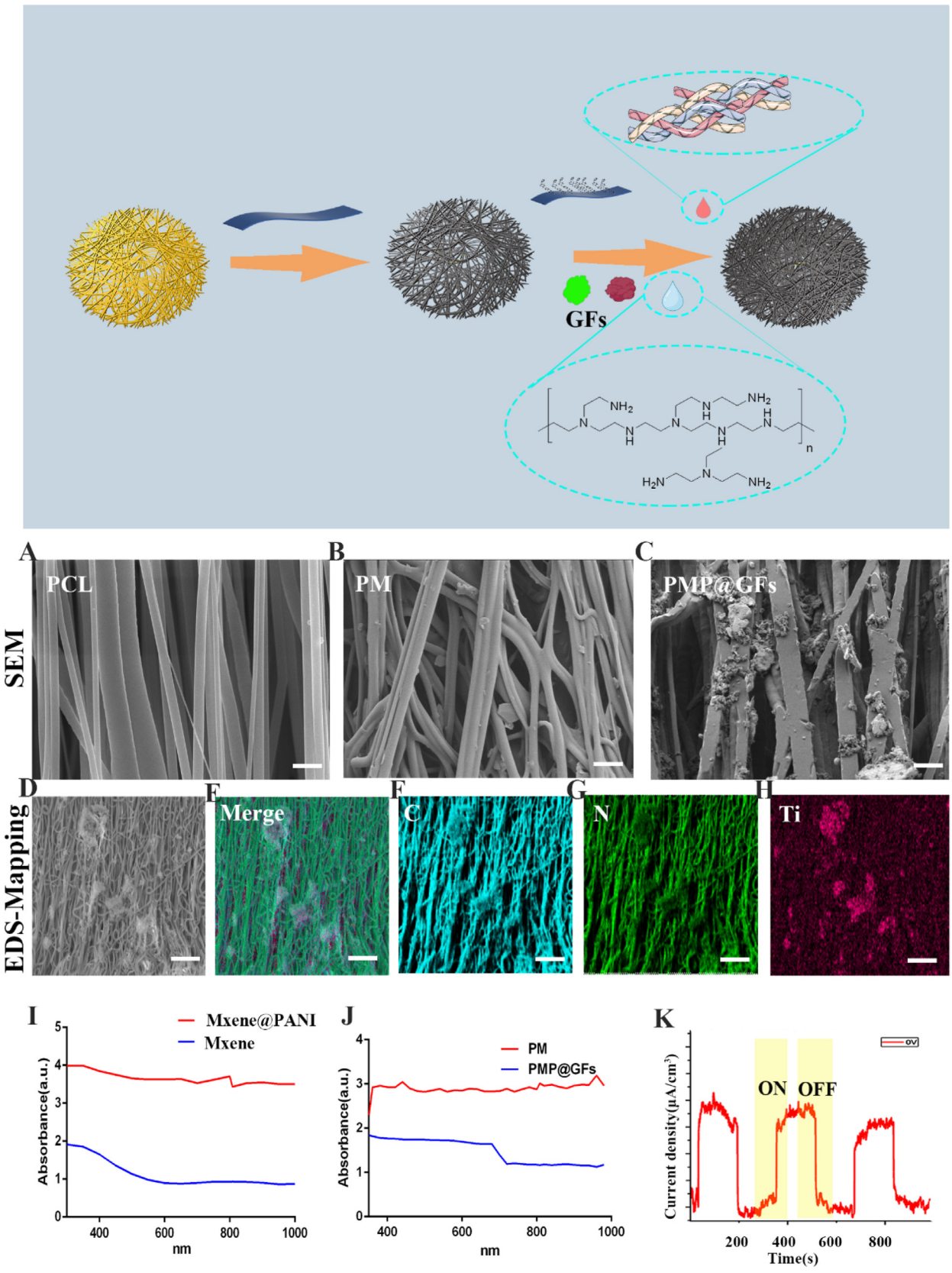

Fig. 2. Characterization of photocatalytic oxygen evolution and antibacterial biomimetic repair membranes (A–C) The scanning electron microscope of PCL/PM/PMP@GFs biomimetic repair membrane. (D–H) The EDS-mapping of PMP@GFs biomimetic repair membrane, (I)Absorption spectrum of MXene and MXene@PANI, (J) Absorption spectrum of PM and PMP@GFs, (K) photoelectric effect of MXene@PANI. Scale bar = 200 μm in panels A–C, Scale bar = 100 μm in panels D–H.

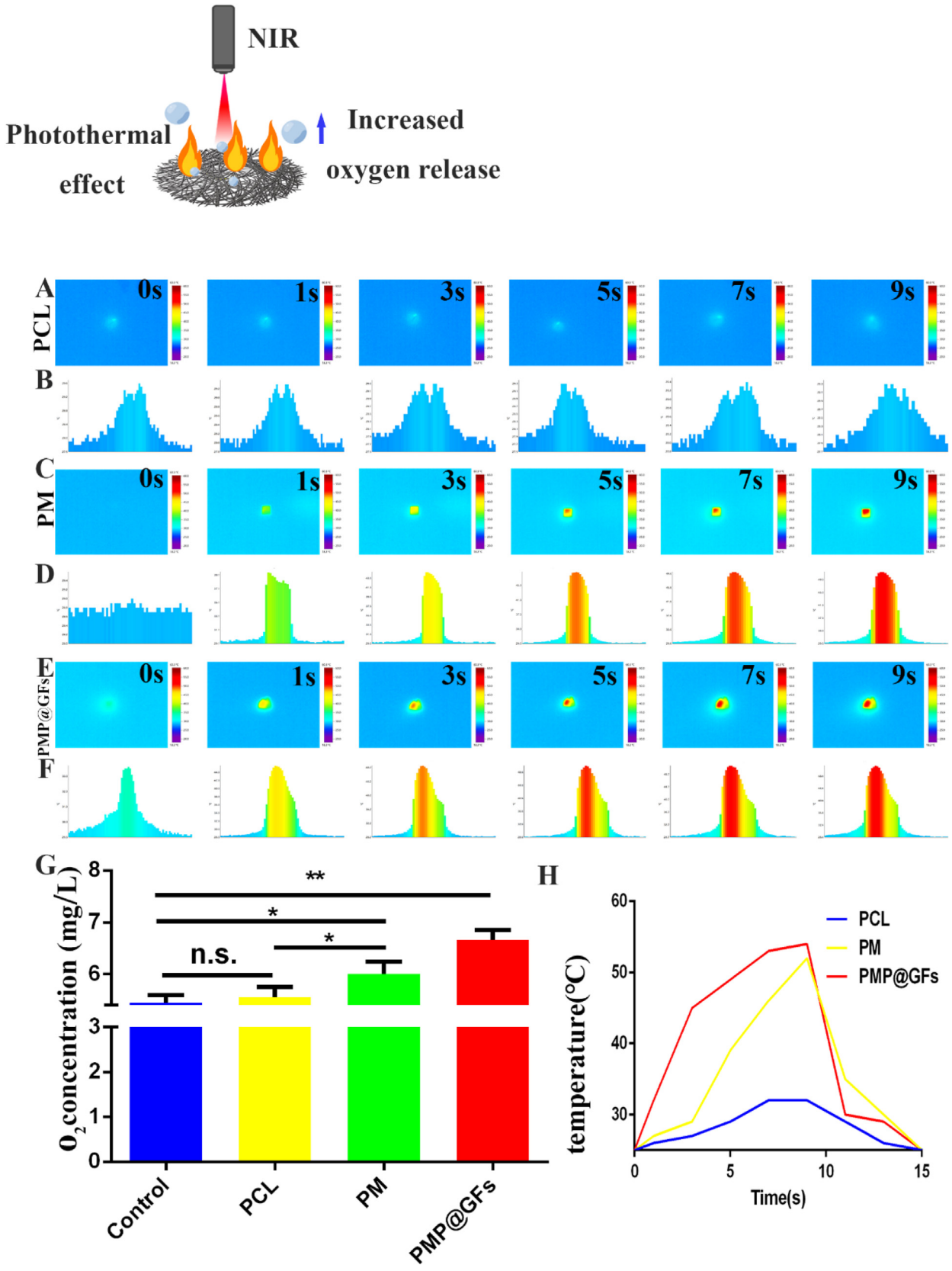

Fig. 3. Photothermal effect and oxygen evolution performance of photocatalytic oxygen evolution and antibacterial biomimetic membranes. (A–F) Photothermal effect and cross-section temperature statistics of PCL/PM/PMP@GFs biomimetic repair membranes. (G) Statistical diagram of oxygen evolution from PCL/PM/PMP@GFs biomimetic repair membranes. (H) A photothermal cycle of CL/PM/PMP@GFs biomimetic membranes. Data represent the mean ± s.d., n = 3, $*p < 0.05$, $**p < 0.01$.

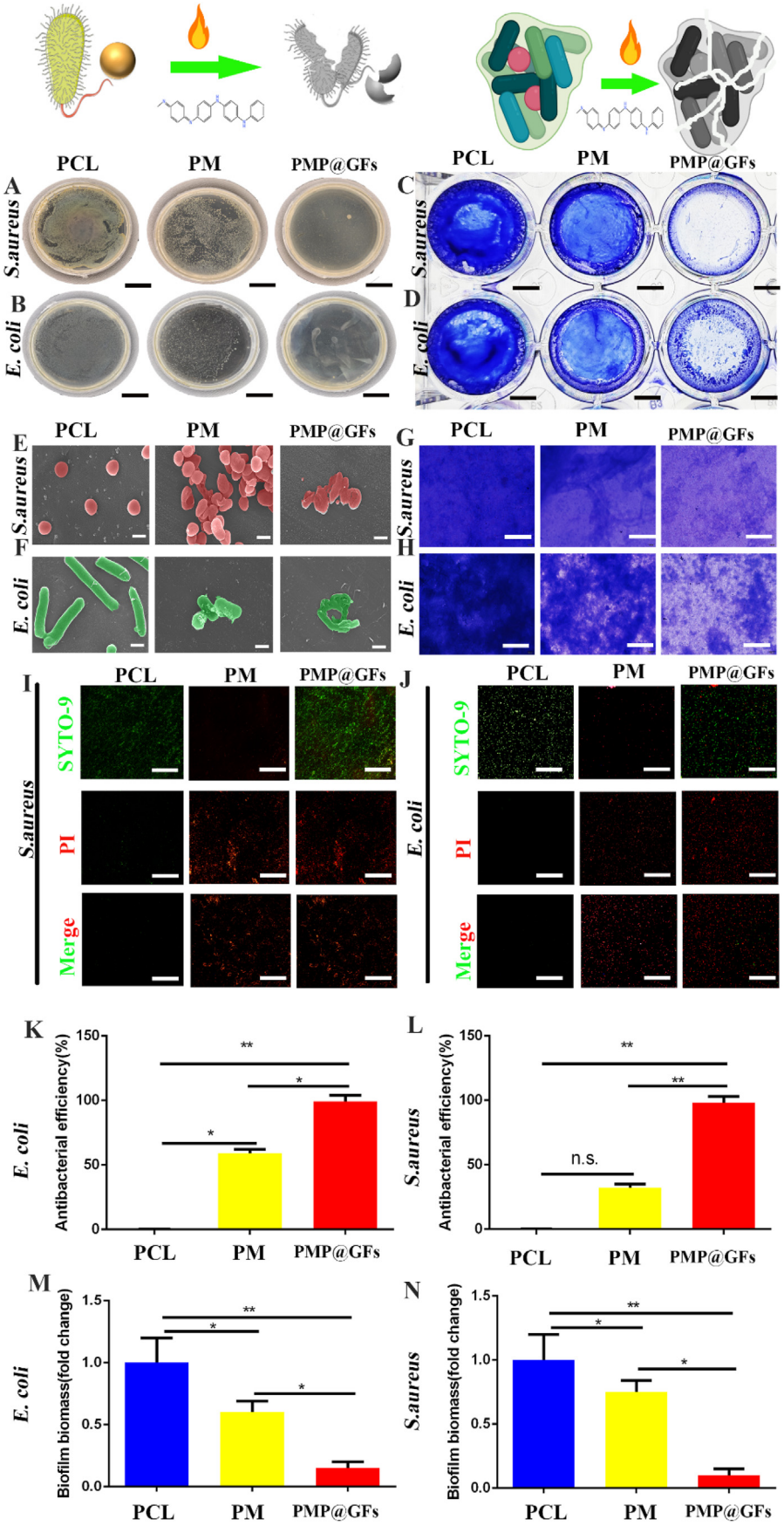

Fig. 4. Antibacterial performance of photocatalytic oxygen evolution and antibacterial biomimetic repair membranes. (A) The anti-Staphylococcus aureus effect of the biomimetic film, (B) The anti-Escherichia coli effect of the biomimetic film, (C) The anti-Staphylococcus aureus biofilm effect of the biomimetic film, (D) The anti-Escherichia coli biofilm effect of the biomimetic film, (E) The scanning electron microscope of the biomimetic film against *Staphylococcus aureus*, (F) The scanning electron microscope of the biomimetic film against *Escherichia coli*, (G) The light microscope of the *Staphylococcus aureus* biofilm, (H) The light microscope of the *Escherichia coli* biofilm, (I) The live death experiment of *Staphylococcus aureus*, (J) The live death experiment of *Escherichia coli*, (K) The statistical diagram of A, (L) The statistical diagram of B, (M) The statistical diagram of C, and (N) The statistical diagram of D. Scale bar = 2 cm in panels A and B, 0.5 cm in panels C and D, 0.5 μm in panels E and F, 200 μm in panels G and H, 100 μm in panels I and J. Data represent the mean ± s.d., n = 3, $*p < 0.05$, $**p < 0.01$.

At the same time, we also observed that the surface of the character *Staphylococcus aureus* in the PM biomimetic membrane group has specific depression (Fig. 4. E). And then, the structure of *Escherichia coli* was destroyed in PMP@GFs, and some damage in PM (Fig. 4. F).

At the same time, we also tested the live/death of bacteria, and we can see whether it is *Escherichia coli* or *Staphylococcus aureus*. Compared with the PCL group, the PMP@GFs bionic membrane group had many dead bacteria (Fig. 4. I, J).

3.4. PMP@GFs biomimetic membranes promote collagen secretion of fibroblasts

Fibroblasts are the dermis' primary cells and play an essential role in the skin wound healing process. Therefore, we first co-culture the biomimetic membrane with fibroblasts.

With the expression of Vimentin in fibroblasts, it can be seen that the PMP@GFs biomimetic membrane group was 2.76 times as much as the PCL group (Fig. 5. A, H). The expression of collagen I in the PMP@GFs Biomimetic membrane group was 2.03 times that of the PCL group (Fig. 5. B, I). For accession of collagen III, PMP@GFs biomimetic membrane group was 4.11 times that of the PCL group (Fig. 5. C, J). To test HIF1-α expressions of fibroblasts. It can be seen that the PMP@GFs Biomimetic membrane group was 1.49 times as much as the PCL group (Fig. 5. D, K). The above results show that the PMP@GFs biomimetic membrane can promote the expression of collagen I and collagen III.

The [Ru (DPP) $_3$] Cl_2 quenches after encountering oxygen, reflecting oxygen content. It can be seen that the fluorescence intensity of the PMP@GFs biomimetic membrane group was 0.59 times that of the PCL group (Fig. 5. E, L). Since oxygen plays a vital role in aerobic respiration, and mitochondria are essential participants, we used a JC-1 kit to detect mitochondrial membrane potential. Mitochondria in PMP@GFs become longer (Fig. 5. F), which may be one of the mechanisms that lead to the enhancement of fibroblast activity and the increase of collagen secretion.

3.5. PMP@GFs biomimetic membrane promotes nerve and blood vessel regeneration in vitro and vivo

Vascular regeneration can mainly transport oxygen and nutrients to the injured area during wound repair. Therefore, the PMP@GFs Biomimetic membrane was co-cultured with HUVECs. It can be seen that the expression of CD31 in the PMP@GFs biomimetic membrane group was 2.09 times higher than that in the PCL group (Fig. 6. A). And the fluorescence intensity of the PMP@GFs biomimetic membrane group was 0.49 times that of the PCL group (Fig. 6. B). Finally, we detected the mitochondria in cells and found that the mitochondria of cells in the PMP@GFs biomimetic membrane group increased significantly, and the fluorescence intensity also increased significantly (Fig. 6. C). The above experiments confirmed that PMP@GFs Biomimetic membrane could enhance vascular endothelial cell activity.

Nerve regeneration is also significant in the process of wound repair. Later, the PMP@GFs Biomimetic membrane was co-cultured in PC12 cells. As shown in the figure, NF200 staining in the PMP@GFs biomimetic membrane group was significantly enhanced, which is 2.87 times that of the PCL group (Fig. 6 D-F). We detected the mitochondria in cells and found that the mitochondria of cells in the PMP@GFs biomimetic membrane group increased significantly, and the fluorescence intensity also increased significantly (Fig. 6. G). The above results show that the PMP@GFs Biomimetic membrane is vital in regulating nerves and blood vessels in wound repair. Mitochondrial morphology of fibroblasts and HUVEC is lengthened, and that of PC12 cells is the most obvious, which indicates that mitochondria of PC12 may play an essential role in oxygen-promoting wound healing of diabetes.

PMP@GFs biomimetic membrane-induced repair and angiogenesis of diabetes wounds. Subsequently, we implanted the biomimetic membrane into the wound site of diabetes rats. The wound-healing effect of the PMP@GFs biomimetic membrane group was the best on the 14th day. The wound area of the PMP@GFs group was significantly smaller than that of the PCL group, which is 0.17 times that of the wound group at the time of implantation (Fig. 7 A-G).

At the same time, the photothermal effect of the PMP@GFs biomimetic membrane after implantation was tested. The biomimetic membrane at the implantation site warmed up fastest, rising to 65 °C in 9 s. The control group only warmed up to 32 °C in the process, and the PCL temperature rise was significantly slower than that of the PMP@GFs biomimetic membrane group (Fig. 7 H-J).

Finally, we performed HE and MASSON staining on the skin repaired by the biomimetic membrane to detect the repair of the wound. From the results, the PMP@GFs biomimetic membrane group can improve the wound surface and has a noticeable repair effect on the dermis and epidermis of the skin (Fig. 7 K-P). It can be seen from the quantitative analysis that the collagen content in the biomimetic membrane group increased significantly, 2.30 times as much as that in the PCL group (Fig. 7. V). We also performed immunofluorescence staining on the vascular endothelium of the wound. We found that the PMP@GFs biomimetic membrane can significantly promote the formation of blood vessels, which is 2.55 times that of the PCL group (Fig. 7. R-T, W). The above results show that the PMP@GFs biomimetic membrane can promote the repair of diabetes wounds and the regeneration of blood vessels in vivo.

4. Discussion

We successfully constructed a photocatalytic oxygen evolution and antibacterial biomimetic membrane in this experiment. In vivo and vitro, we confirmed that the biomimetic membrane has apparent oxygen production and antibacterial activity. It can promote the healing of diabetic wounds. This will provide a promising treatment way for diabetic wounds.

The main features of diabetic wounds included hypoxia and infection [4,37], which were the two main obstacles leading to poor wound healing. Relieving chronic hypoxia of skin cells is beneficial to diabetic wound healing. At present, there are many materials to treat the poor healing of diabetic wounds caused by bacteria and other factors [38–41]. Oxygen therapy was superior to drug therapy because of its favorable safety [34]. The infection caused neutrophils to secrete reactive oxygen species to destroy bacteria. The production of reactive oxygen species required molecular oxygen, further leading to local cell hypoxia [2]. We construct the heterojunction structure with MXene and PANI. The wealthy functional groups produced by MXene in the wet chemical etching process form a close contact interface with PANI. The conductive metal core in the layered structure gives MXene excellent electron acceptance ability. This also made MXene have remarkable photocatalytic activity [42]. On the other hand, PANI could improve the carrier migration efficiency at the interface between PANI and MXene and improve photocatalytic performance [25]. Based on our assumptions, we first explored the effect of oxygen released by biomimetic membranes on the viability of cells in an anoxic environment. The results showed that under hypoxia, the survival rate of nerve cells, fibroblasts, epidermal cells, and endothelial cells increased significantly with the oxygen released by a biomimetic membrane. These cell types were responsible for nerve regeneration, epithelialization, wound contraction, and angiogenesis. Intracellular oxygen is essential for mitochondrial metabolism. Hypoxic levels of local cells caused by diabetic wounds impaired this process [43]. Due to the relief of hypoxia, we found that the mitochondria of wound local damage in the PMP@GFs biomimetic membrane group were significantly increased. In previous studies, biocompatibility was critical in applying materials in vivo [44].

Photothermal therapy (PTT) is a safe and effective strategy for treating infection and promoting tissue regeneration. Near-infrared light has a favorable ability to penetrate the body of mammals with damage to normal tissues. Hyperthermia inhibits bacteria's growth and mild heat and promotes cell proliferation. It played a positive role in wound healing

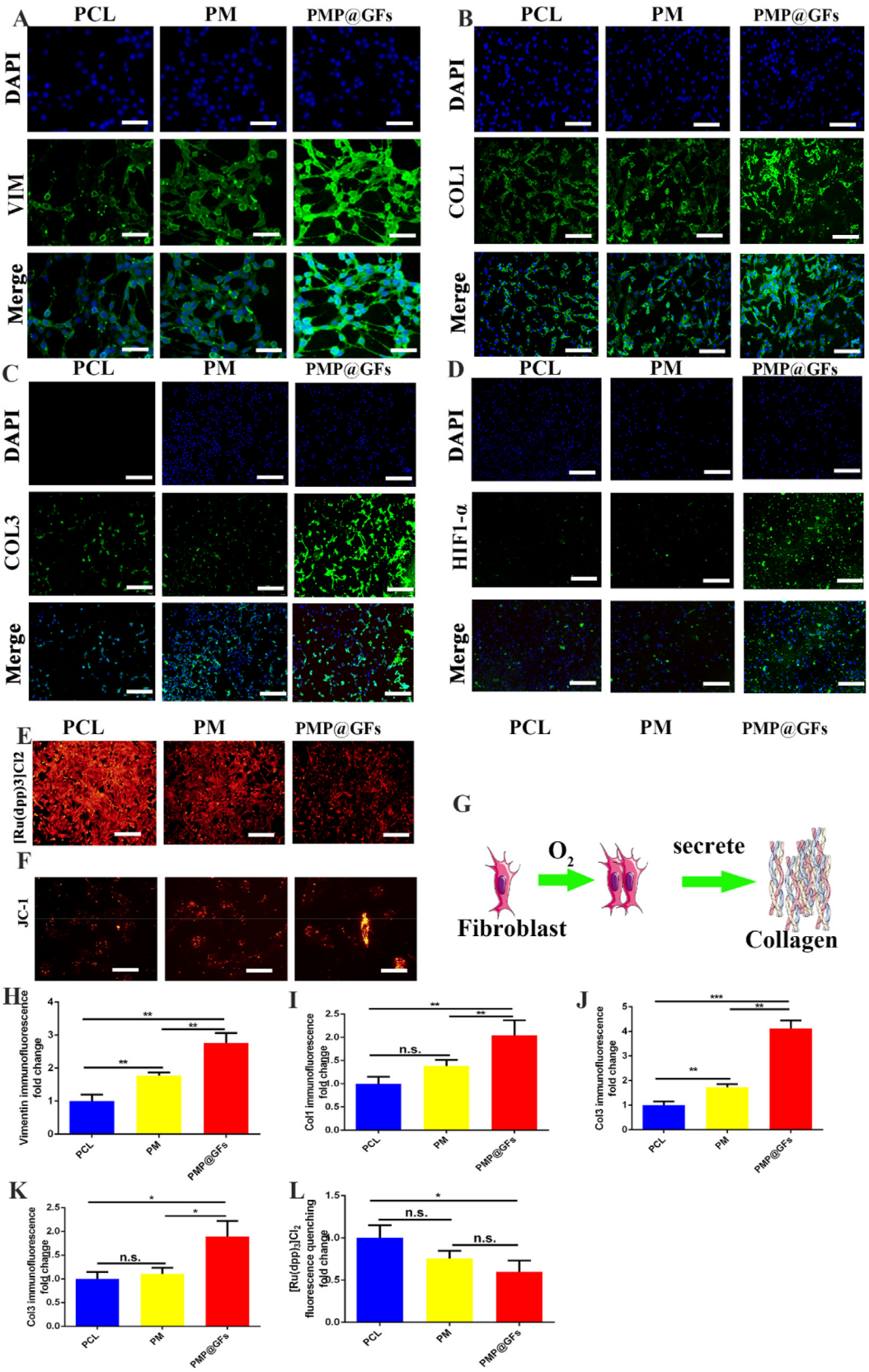

Fig. 5. Photocatalytic oxygen evolution and antibacterial biompromoteepair membrane promote collagen secretion by fibroblasts. (A) The immunofluorescence staining of fibroblast marker Vimentin, (B) The immunofluorescence staining of fibroblasts expressing collagen I, (C) The immunofluorescence staining of fibroblasts expressing collagen III, and (D) The HIF1 of fibroblasts- α. (E) The detection of the oxygen content of fibroblasts. (F) The mitochondrial membrane potential detection of fibroblasts, (G) The pattern diagram of collagen secretion by fibroblasts, (H) The statistical diagram of A, (I) The statistical diagram of B, (J) The statistical diagram of C, (K) The statistical diagram of D, and (L) The statistical diagram of F. Scale bar = 100 μm in panel A, 200 μm in panels B–E, 50 μm in panel F. Data represent the mean ± s.d., n = 3, $*p < 0.05$, $**p < 0.01$, $***p < 0.001$.

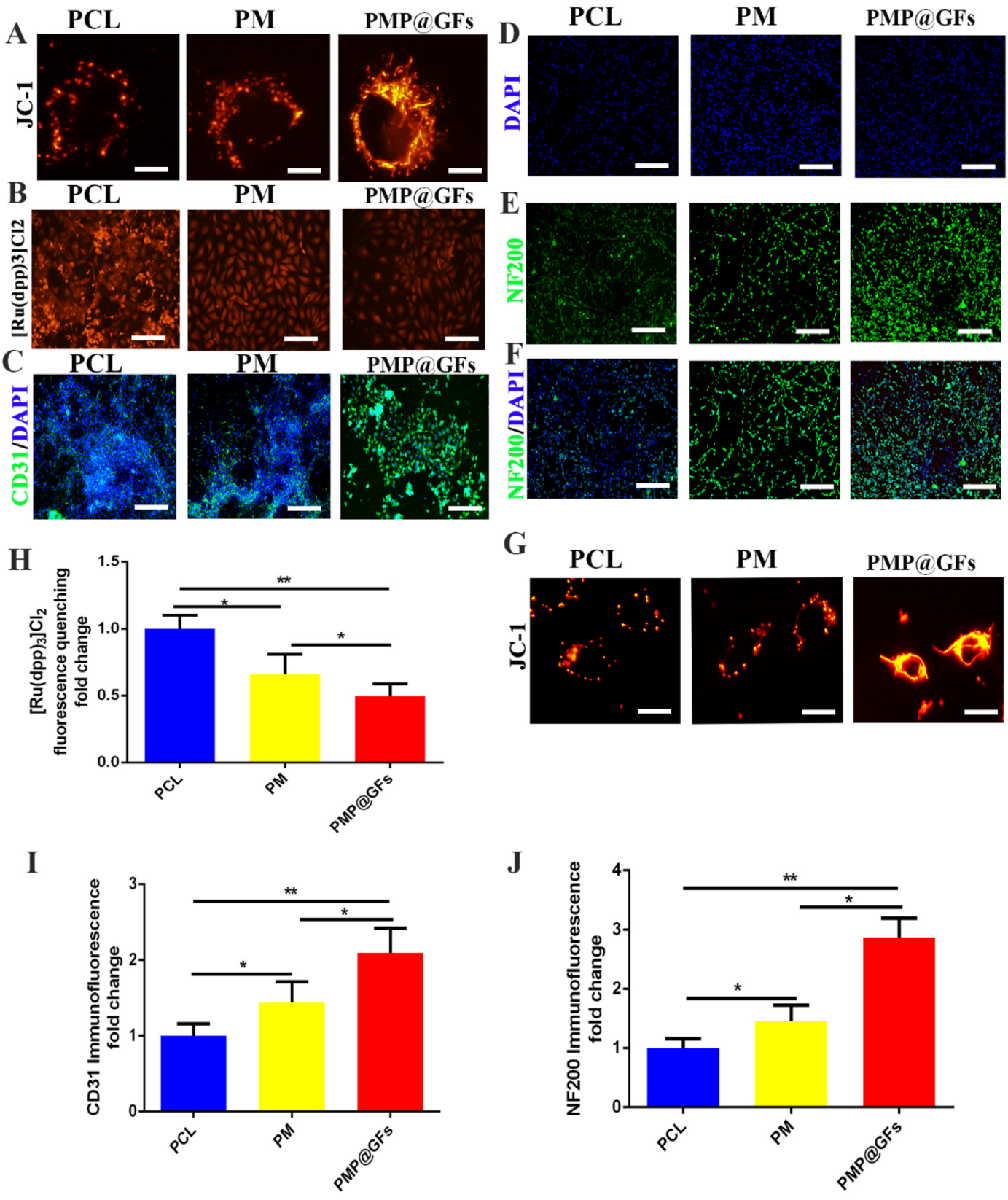

Fig. 6. Photocatalytic oxygen evolution and antibacterial biomimetic repair membrane promote the activity of HUVEC and PC12. (A) The mitochondrial membrane potential staining of HUVEC, (B) The oxygen detection of HUVEC, (C) The CD31 immunofluorescence staining of HUVEC, (D–F) The NF200 immunofluorescence staining of PC12, (G) The mitochondrial membrane potential of PC12, (H) The statistical diagram of B, (I) The statistical diagram of C, and (J) The statistical diagram of E. Scale bar = 20 μm in panels A and G, 200 μm in panels B–F. Data represent the mean ± s.d., n = 3, $^{*}p < 0.05$, $^{**}p < 0.01$.

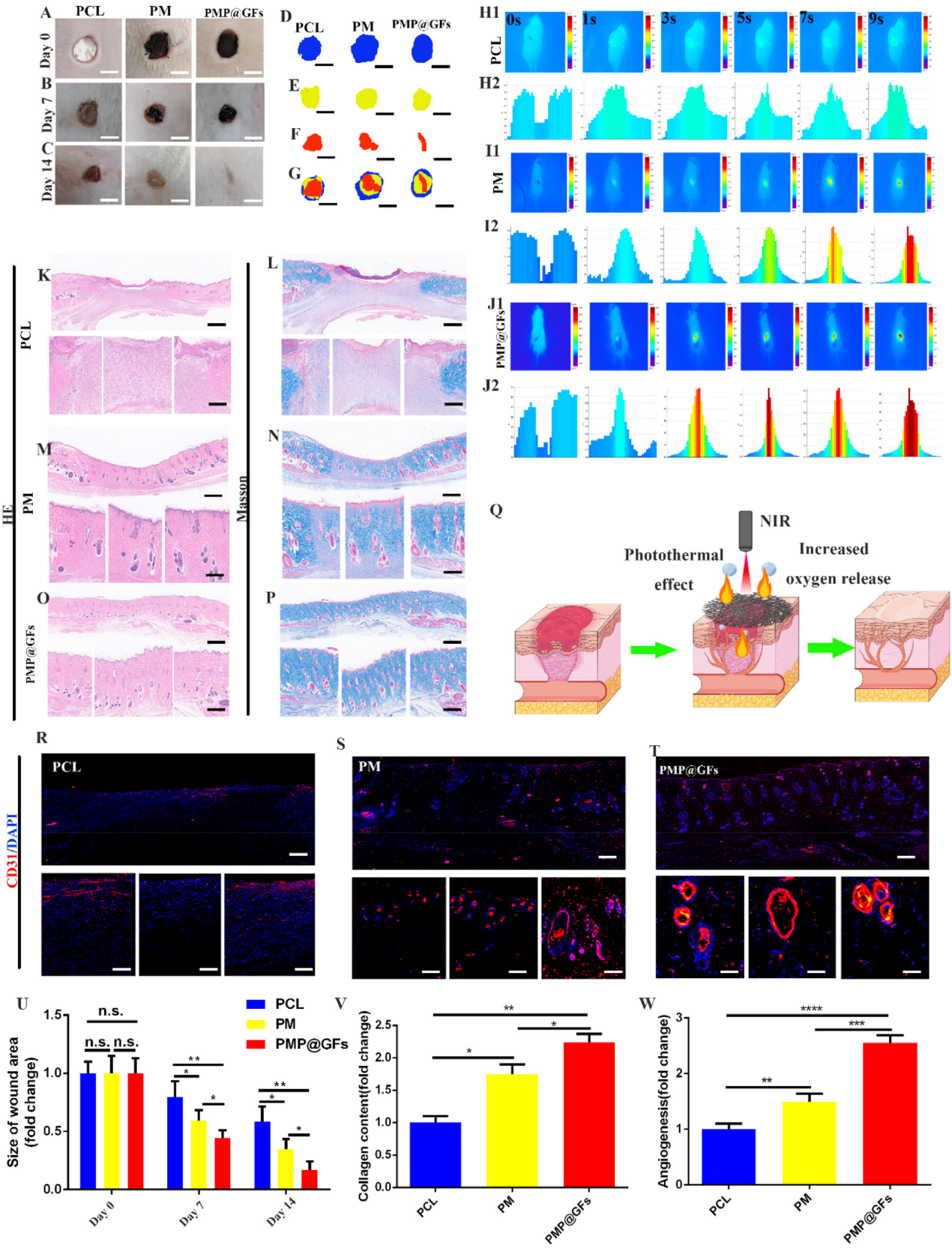

Fig. 7. Photocatalytic oxygen evolution and antibacterial biomimetic repair membrane promote the repair of diabetes wounds in vivo. (A–C) The recovery of the wound in rats, (D–F) The contour of the wound, (G) The composite contour of different periods, (H–J) The photo of the photothermal effect in vivo of the bionic membrane. (K, M, O) The HE detection of the bionic membrane repair wound. (L, N, P) The MASSON detection of the bionic membrane repair wound, (Q) PMP@GFs The model diagram of biomimetic membrane treatment of diabetes wound. (R–T) CD31 immunofluorescence staining of the wound, (U) The statistical diagram of A. (V) The statistical diagram of L, N, P. (W) The statistical diagram of R-T. Scale bar = 5 cm in panels A–C, 200 μm and 100 μm in panels K–P, R-T. Data represent the mean ± s.d., n = 3, $*p < 0.05$, $**p < 0.01$, $***p < 0.001$, $****p < 0.0001$.

[45,46]. Previous research reports showed that PANI materials have excellent photothermal-friendly conversion efficiency [47,48]. However, only sommeliers combined the two materials and tested their photothermal efficiency. Therefore, we further explored the biomimetic membrane's photothermal efficiency and antibacterial ability. An essential criterion for PTT treatment was temperature. When the temperature exceeded 50 °C, most bacteria were killed due to membrane rupture [49–52]. We evaluate the photothermal properties of the membrane between the PCL and PMP@GFs biomimetic membrane after being irradiated with a near-infrared laser at 808 nm. In in vivo and vitro, we found that the temperature of our PMP@GFs biomimetic membrane could rise rapidly to above 50 °C in 9 s. Then, we evaluated the repeat biomimetic membrane's repeatable near-infrared photothermal properties. The results show that the biomimetic membrane has good photothermal conversion efficiency and photothermal effect of observing the tutorial effect of PMP@GFs biomimetic membrane. *Staphylococcus aureus* and *Escherichia coli* were co-cultured with biomimetic membranes. The general observation, in vivo death test, and scanning electron microscope show that the bionic membrane can effectively kill more than 95% of the bacteria. At the same time as effective sterilization, it also has an apparent inapparent effect on bacterial biofilm.

We conducted in vivo experiments to get further convincing evidence. We made a diabetic mouse model and a circular wound defect with a radius of 5 mm. Then the biomimetic membrane was covered on the wound defect. We found that the biomimetic membrane significantly repaired the dermis and epidermis of diabetic rats. The regeneration of blood vessels in the wound was one of the necessary conditions for repairing and regenerating the dermis [53]. It was demonstrated that VEGF encapsulated by PEI was well released in the acidic environment of diabetes. The joint action of VEGF and MXene significantly promoted angiogenesis. The photothermal efficiency and antibacterial ability in vivo had also been well verified. Under the irradiation of near-infrared light, the biomimetic membrane had an exciting photothermal conversion efficiency in vivo, reaching 65 °C in 9 s and falling to the actual temperature in 6 s. The experimental results in vivo showed that the photocatalytic biomimetic repair membrane significantly promoted the wound healing of diabetic rats. The biomimetic repair membrane implanted into the wound of diabetic rats has the functions of oxygen production and antibacterial.

In brief, our experiments fully demonstrated that the biomimetic repair membrane with multiple functions, including photocatalytic oxygen evolution and antibacterial, promoting vascular regeneration and effectively accelerating the healing of diabetic wounds. According to the exciting experimental results, we provide a new scheme for diabetic wound healing. This new material has great potential for clinical application. Moreover, we are optimistic that our materials have potential applications in infectious bone defects, odontogenic infections, and other diseases. We will further promote the experiment and make our materials play a better role.

5. Conclusions

We have successfully constructed photocatalytic oxygen evolution and antibacterial biomimetic repair membranes (PMP@GFs) to treat diabetic wounds. The experiments above confirmed that the PMP@GFs biomimetic repair membrane could release oxygen under near-infrared irradiation and eliminate bacteria in the wound by the photothermal effect. In vitro, the biomimetic repair membrane can promote the activity of fibroblasts, vascular endothelial cells, and nerve cells. In vivo, the biomimetic repair membrane can release growth factors, including VEGF and NGF, to promote the regeneration of blood vessels and nerves and finally achieve the role of promoting wound repair. The photocatalytic oxygen evolution and antibacterial biomimetic repair membrane provide a new and promising treatment method for repairing diabetes wounds.

Credit author statement

Yanlin Su, Bing Ye, Ziming Zhang: conceptualization, data curation, methodology, writing—original draft preparation, writing—review, and editing; Qing Gao: software, data curation, methodology; Lian Zeng, Yizhou Wan, Wenzhe Sun: conceptualization, methodology; Siyue Chen: Validation, Visualization; Daping Quan, Jialin Yu, Xiaodong Guo: conceptualization, writing—review and editing, supervision, project administration. All authors have read and agreed to the published version of the manuscript.

Funding

This work was financially supported by the National Natural Science Foundation of China (82072446) (81873999), the Introduction plan of high-end foreign experts of the Ministry of science and technology of China (G2021154012L), and the natural science foundation of Hubei Province (2020BCB050).

Declaration of competing interest

The authors declare that they have no known competing financial interests or personal relationships that could have appeared to influence the work reported in this paper.

Data availability

Data will be made available on request.

Acknowledgments

Thank the analysis and testing center of Huazhong University of Science and Technology for its support. Thanks to the funding support from the National Natural Science Foundation of China. The schematic diagram in each figure is created by BioRender.com and smart.

References

[1] S. Maschalidi, P. Me hrotra, B.N. Keceli, H.K.L. De Cleene, K. Lecomte, R. Van der Cruyssen, P. Janssen, J. Pinney, G. van Loo, D. Elewaut, A. Massie, E. Hoste, K.S. Ravichandran, Targeting SLC7A11 improves efferocytosis by dendritic cells and wound healing in diabetes, Nature 606 (2022) 776–784, https://doi.org/10.1038/s41586-022-04754-6.

[2] M. Chang, T.T. Nguyen, Strategy for treatment of infected diabetic foot ulcers, Acc. Chem. Res. 54 (2021) 1080–1093, https://doi.org/10.1021/acs.accounts.0c00864.

[3] J.L. Burgess, W.A. Wyant, B. Abdo Abujamra, R.S. Kirsner, I. Jozic, Diabetic wound-healing science, Medicina 57 (2021) 1072, https://doi.org/10.3390/medicina57101072.

[4] J.J. Li, Y. Hu, B. Hu, W. Wang, H. Xu, X.Y. Hu, F. Ding, H.B. Li, K.R. Wang, X. Zhang, D.S. Guo, Lactose azocalixarene drug delivery system for the treatment of multidrug-resistant pseudomonas aeruginosa infected diabetic ulcer, Nat. Commun. 13 (2022) 6279, https://doi.org/10.1038/s41467-022-33920-7.

[5] Z. Li, X. Fan, Z. Luo, X.J. Loh, Y. Ma, E. Ye, Y.L. Wu, C. He, Z. Li, Nanoenzyme-chitosan hydrogel complex with cascade catalytic and self-reinforced antibacterial performance for accelerated healing of diabetic wounds, Nanoscale 14 (2022) 14970–14983, https://doi.org/10.1039/d2nr04171e.

[6] A. Agrawal, U. Mabalirajan, Rejuvenating cellular respiration for optimizing respiratory function: targeting mitochondria, Am. J. Physiol. Lung Cell Mol. Physiol. 310 (2016) 103–113, https://doi.org/10.1152/ajplung.00320.2015.

[7] X. Hong, J. Isern, S. Campanario, E. Perdiguero, I. Ramirez-Pardo, J. Segales, P. Hernansanz-Agustin, A. Curtabbi, O. Deryagin, A. Pollan, J.A. Gonzalez-Reyes, J.M. Villalba, M. Sandri, A.L. Serrano, J.A. Enriquez, P. Munoz-Canoves, Mitochondrial dynamics maintain muscle stem cell regenerative competence throughout adult life by regulating metabolism and mitophagy, Cell Stem Cell 29 (2022) 1506–1508, https://doi.org/10.1016/j.stem.2022.09.002.

[8] A. Tanaka, R.J. Youle, A chemical inhibitor of DRP1 uncouples mitochondrial fission and apoptosis, Mol. Cell. 29 (2008) 409–410, https://doi.org/10.1016/j.molcel.2008.02.005.

[9] H. Wu, F. Li, W. Shao, J. Gao, D. Ling, Promoting angiogenesis in oxidative diabetic wound microenvironment using a nanozyme-reinforced self-protecting hydrogel, ACS Cent. Sci. 5 (2019) 477–485, https://doi.org/10.1021/acscentsci.8b00850.

[10] L.M. Frydrych, G. Bian, D.E. O'Lone, P.A. Ward, M.J. Delano, Obesity and type 2 diabetes mellitus drive immune dysfunction, infection development, and sepsis

mortality, J. Leukoc. Biol. 104 (2018) 525–534, https://doi.org/10.1002/jlb.5vmr0118-021rr.
[11] C. Tu, H. Lu, T. Zhou, W. Zhang, L. Deng, W. Cao, Z. Yang, Z. Wang, X. Wu, J. Ding, F. Xu, C. Gao, Promoting the healing of infected diabetic wound by an anti-bacterial and nano-enzyme-containing hydrogel with inflammation-suppressing, ROS-scavenging, oxygen and nitric oxide-generating properties, Biomaterials 286 (2022), 121597, https://doi.org/10.1016/j.biomaterials.2022.121597.
[12] T. Wang, Y. Li, E.J. Cornel, C. Li, J. Du, Combined antioxidant-antibiotic treatment for effectively healing infected diabetic wounds based on polymer vesicles, ACS Nano 15 (2021) 9027–9038, https://doi.org/10.1021/acsnano.1c02102.
[13] P.L. Thi, Y. Lee, D.L. Tran, T.T.H. Thi, J.I. Kang, K.M. Park, K.D. Park, In situ forming and reactive oxygen species-scavenging gelatin hydrogels for enhancing wound healing efficacy, Acta Biomater. 103 (2020) 142–152, https://doi.org/10.1016/j.actbio.2019.12.009.
[14] Y. Zhang, J. Tan, Y. Miao, Q. Zhang, The effect of extracellular vesicles on the regulation of mitochondria under hypoxia, Cell Death Dis. 12 (2021) 358, https://doi.org/10.1038/s41419-021-03640-9.
[15] C. Tong, X. Zhong, Y. Yang, X. Liu, G. Zhong, C. Xiao, B. Liu, W. Wang, X. Yang, PB@PDA@Ag nanosystem for synergistically eradicating MRSA and accelerating diabetic wound healing assisted with laser irradiation, Biomaterials 243 (2020), 119936, https://doi.org/10.1016/j.biomaterials.2020.119936.
[16] G. Duan, L. Wen, X. Sun, Z. Wei, R. Duan, J. Zeng, J. Cui, C. Liu, Z. Yu, X. Xie, M. Gao, Healing diabetic ulcers with MoO_{3-X} nanodots possessing intrinsic ROS-scavenging and bacteria-killing capacities, Small 18 (2022), e2107137, https://doi.org/10.1002/smll.202107137.
[17] N.C. Nowak, D.M. Menichella, R. Miller, A.S. Paller, Cutaneous innervation in impaired diabetic wound healing, Transl. Res. 236 (2021) 87–108, https://doi.org/10.1016/j.trsl.2021.05.003.
[18] S.T. Krishnan, C. Quattrini, M. Jeziorska, R.A. Malik, G. Rayman, Neurovascular factors in wound healing in the foot skin of type 2 diabetic subjects, Diabetes Care 30 (2007) 3058–3062, https://doi.org/10.2337/dc07-1421.
[19] C. Quattrini, M. Jeziorska, A.J. Boulton, R.A. Malik, Reduced vascular endothelial growth factor expression and intra-epidermal nerve fiber loss in human diabetic neuropathy, Diabetes Care 31 (2008) 140–145, https://doi.org/10.2337/dc07-1556.
[20] H. Galkowska, W.L. Olszewski, U. Wojewodzka, G. Rosinski, W. Karnafel, Neurogenic factors in the impaired healing of diabetic foot ulcers, J. Surg. Res. 134 (2006) 252–258, https://doi.org/10.1016/j.jss.2006.02.006.
[21] X. Zhao, L.Y. Wang, J.M. Li, L.M. Peng, C.Y. Tang, X.J. Zha, K. Ke, M.B. Yang, B.H. Su, W. Yang, Redox-mediated artificial non-enzymatic antioxidant MXene nanoplatforms for acute kidney injury alleviation, Adv. Sci. 8 (2021), e2101498, https://doi.org/10.1002/advs.202101498.
[22] R. Li, L. Zhang, L. Shi, P. Wang, MXene Ti(3)C(2): an effective 2D light-to-heat conversion material, ACS Nano 11 (2017) 3752–3759, https://doi.org/10.1021/acsnano.6b08415.
[23] A.M. Jastrzebska, A. Szuplewska, T. Wojciechowski, M. Chudy, W. Ziemkowska, L. Chlubny, A. Rozmyslowska, A. Olszyna, In vitro studies on cytotoxicity of delaminated Ti(3)C(2) MXene, J. Hazard Mater. 339 (2017) 1–8, https://doi.org/10.1016/j.jhazmat.2017.06.004.
[24] H. Lin, S. Gao, C. Dai, Y. Chen, J. Shi, A two-dimensional biodegradable niobium carbide (MXene) for photothermal tumor eradication in NIR-I and NIR-II biowindows, J. Am. Chem. Soc. 139 (2017) 16235–16247, https://doi.org/10.1021/jacs.7b07818.
[25] H. Lin, Y. Wang, S. Gao, Y. Chen, J. Shi, Theranostic 2D tantalum carbide (MXene), Adv. Mater. 30 (2018), https://doi.org/10.1002/adma.201703284.
[26] K. Rasool, K.A. Mahmoud, D.J. Johnson, M. Helal, G.R. Berdiyorov, Y. Gogotsi, Efficient antibacterial membrane based on two-dimensional $Ti_3C_2T_x$ (MXene) nanosheets, Sci. Rep. 7 (2017) 1598, https://doi.org/10.1038/s41598-017-01714-3.
[27] P. Kuang, J. Low, B. Cheng, J. Yu, J. Fan, MXene-based photocatalysts, J. Mater. Sci. Technol. 56 (2020) 18–44, https://doi.org/10.1016/j.jmst.2020.02.037.
[28] L. Zhou, H. Zheng, Z. Liu, S. Wang, Z. Liu, F. Chen, H. Zhang, J. Kong, F. Zhou, Q. Zhang, Conductive antibacterial hemostatic multifunctional scaffolds based on $Ti_3C_2T_x$ MXene nanosheets for promoting multidrug-resistant bacteria-infected wound healing, ACS Nano 15 (2021) 2468–2480, https://doi.org/10.1021/acsnano.0c06287.
[29] S. Liu, D. Li, Y. Wang, G. Zhou, K. Ge, L. Jiang, D. Fang, Flexible, high-strength and multifunctional polyvinyl alcohol/MXene/polyaniline hydrogel enhancing skin wound healing, Biomater. Sci. 10 (2022) 3585–3596, https://doi.org/10.1039/d2bm00575a.
[30] S. Sharma, S. Singh, N. Khare, Enhanced photosensitization of zinc oxide nanorods using polyaniline for efficient photocatalytic and photoelectrochemical water splitting, Int. J. Hydrogen Energy 41 (2016) 21088–21098, https://doi.org/10.1016/j.ijhydene.2016.08.131.
[31] H.S. Kushwaha, P. Thomas, R. Vaish, Polyaniline/CaCu3Ti4O12 nanofiber composite with a synergistic effect on visible light photocatalysis, RSC Adv. 5 (2015) 87241–87250, https://doi.org/10.1039/c5ra16518k.
[32] L. Liu, L. Ding, Y. Liu, W. An, S. Lin, Y. Liang, W. Cui, A stable Ag3PO4@PANI core@shell hybrid: enrichment photocatalytic degradation with π-π conjugation, Appl. Catal., B 201 (2017) 92–104, https://doi.org/10.1016/j.apcatb.2016.08.005.
[33] D. Kong, Y. Zheng, M. Kobielusz, Y. Wang, Z. Bai, W. Macyk, X. Wang, J. Tang, Recent advances in visible light-driven water oxidation and reduction in suspension systems, Mater. Today 21 (2018) 897–924, https://doi.org/10.1016/j.mattod.2018.04.009.
[34] Y. Guan, H. Niu, Z. Liu, Y. Dang, J. Shen, M. Zayed, L. Ma, J. Guan, Sustained oxygenation accelerates diabetic wound healing by promoting epithelialization and angiogenesis and decreasing inflammation, Sci. Adv. 7 (2021), https://doi.org/10.1126/sciadv.abj0153 eabj0153.
[35] M. Naguib, M. Kurtoglu, V. Presser, J. Lu, J. Niu, M. Heon, L. Hultman, Y. Gogotsi, M.W. Barsoum, Two-dimensional nanocrystals produced by exfoliation of Ti3 AlC2, Adv. Mater. 23 (2011) 4248–4253, https://doi.org/10.1002/adma.201102306.
[36] B. Anasori, M.R. Lukatskaya, Y. Gogotsi, 2D metal carbides and nitrides (MXenes) for energy storage, Nat. Rev. Mater. 2 (2017), https://doi.org/10.1038/natrevmats.2016.98.
[37] Y. Liang, M. Li, Y. Yang, L. Qiao, H. Xu, B. Guo, pH/glucose dual responsive metformin release hydrogel dressings with adhesion and self-healing via dual-dynamic bonding for athletic diabetic foot wound healing, ACS Nano 16 (2022) 3194–3207, https://doi.org/10.1021/acsnano.1c11040.
[38] X. Ren, Y. Hu, L. Chang, S. Xu, X. Mei, Z. Chen, Electrospinning of antibacterial and anti-inflammatory Ag@hesperidin core-shell nanoparticles into nanofibers used for promoting infected wound healing, Regen. Biomater. 9 (2022), https://doi.org/10.1093/rb/rbac012 rbac012.
[39] X. Zhao, L. Chang, Y. Hu, S. Xu, Z. Liang, X. Ren, X. Mei, Z. Chen, Preparation of photocatalytic and antibacterial MOF nanozyme used for infected diabetic wound healing, ACS Appl. Mater. Interfaces 14 (2022) 18194–18208, https://doi.org/10.1021/acsami.2c03001.
[40] Y. Qian, Y. Zheng, J. Jin, X. Wu, K. Xu, M. Dai, Q. Niu, H. Zheng, X. He, J. Shen, Immunoregulation in diabetic wound repair with a photoenhanced glycyrrhizic acid hydrogel scaffold, Adv. Mater. 34 (2022), e2200521, https://doi.org/10.1002/adma.202200521.
[41] X. He, L. Dai, L. Ye, X. Sun, O. Enoch, R. Hu, X. Zan, F. Lin, J. Shen, A vehicle-free antimicrobial polymer hybrid gold nanoparticle as synergistically therapeutic platforms for Staphylococcus aureus infected wound healing, Adv. Sci. 9 (2022), e2105223, https://doi.org/10.1002/advs.202105223.
[42] Z. Li, Y. Wu, 2D early transition metal carbides (MXenes) for catalysis, Small 15 (2019), e1804736, https://doi.org/10.1002/smll.201804736.
[43] A. Sendoel, M.O. Hengartner, Apoptotic cell death under hypoxia, Physiology 29 (2014) 168–176, https://doi.org/10.1152/physiol.00016.2013.
[44] M. Rahmati, E.A. Silva, J.E. Reseland, A.H. C, H.J. Haugen, Biological responses to physicochemical properties of biomaterial surface, Chem. Soc. Rev. 49 (2020) 5178–5224, https://doi.org/10.1039/d0cs00103a.
[45] G. Guan, K.Y. Win, X. Yao, W. Yang, M.Y. Han, Plasmonically modulated gold nanostructures for photothermal ablation of bacteria, Adv. Healthc. Mater. 10 (2021), e2001158, https://doi.org/10.1002/adhm.202001158.
[46] X. Zhang, G. Cheng, X. Xing, J. Liu, Y. Cheng, T. Ye, Q. Wang, X. Xiao, Z. Li, H. Deng, Near-infrared light-triggered porous AuPd alloy nanoparticles to produce mild localized heat to accelerate bone regeneration, J. Phys. Chem. Lett. 10 (2019) 4185–4191, https://doi.org/10.1021/acs.jpclett.9b01735.
[47] H. Huang, R. Jiang, Y. Feng, H. Ouyang, N. Zhou, X. Zhang, Y. Wei, Recent development and prospects of surface modification and biomedical applications of MXenes, Nanoscale 12 (2020) 1325–1338, https://doi.org/10.1039/c9nr07616f.
[48] J.W. Li, Y. Zhou, J. Xu, F. Gao, Q.K. Si, J.Y. Wang, F. Zhang, L.P. Wang, Water-soluble and degradable gelatin/polyaniline assemblies with a high photothermal conversion efficiency for pH-switchable precise photothermal therapy, ACS Appl. Mater. Interfaces 14 (2022) 52670–52683, https://doi.org/10.1021/acsami.2c16480.
[49] Y. Wang, H.M. Meng, Z. Li, Near-infrared inorganic nanomaterial-based nanosystems for photothermal therapy, Nanoscale 13 (2021) 8751–8772, https://doi.org/10.1039/d1nr00323b.
[50] X. He, J.T. Hou, X. Sun, P. Jangili, J. An, Y. Qian, J.S. Kim, J. Shen, NIR-II photo-amplified sonodynamic therapy using sodium molybdenum bronze nanoplatform against subcutaneous Staphylococcus aureus infection, Adv. Funct. Mater. 32 (2022), https://doi.org/10.1002/adfm.202203964.
[51] S. Huang, S. Xu, Y. Hu, X. Zhao, L. Chang, Z. Chen, X. Mei, Preparation of NIR-responsive, ROS-generating and antibacterial black phosphorus quantum dots for promoting the MRSA-infected wound healing in diabetic rats, Acta Biomater. 137 (2022) 199–217, https://doi.org/10.1016/j.actbio.2021.10.008.
[52] S. Xu, L. Chang, Y. Hu, X. Zhao, S. Huang, Z. Chen, X. Ren, X. Mei, Tea polyphenol modified, photothermal responsive and ROS generative black phosphorus quantum dots as nanoplatforms for promoting MRSA infected wounds healing in diabetic rats, J. Nanobiotechnol. 19 (2021) 362, https://doi.org/10.1186/s12951-021-01106-w.
[53] X. Jin, Y. Shang, Y. Zou, M. Xiao, H. Huang, S. Zhu, N. Liu, J. Li, W. Wang, P. Zhu, Injectable hypoxia-induced conductive hydrogel to promote diabetic wound healing, ACS Appl. Mater. Interfaces 12 (2020) 56681–56691, https://doi.org/10.1021/acsami.0c13197.